Structural Chemistry
https://doi.org/10.1007/s11224-025-02631-2

RESEARCH

Triply periodic surfaces based on metal-organic frameworks

Mikhail I. Smolkov[1,2] · Ekaterina O. Bukhteeva[1] · Ekaterina D. Barabanova[1] · Alexander F. Krutov[1] · Vladislav A. Blatov[1]

Received: 21 August 2025 / Accepted: 26 September 2025

Abstract
With our previously developed method, we generated triply periodic surfaces (TPSs) including 131 minimal surfaces (TPMSs) using crystal structures of 923 metal-organic frameworks (MOFs) as templates. Our approach is based on the topological representation of a MOF structure as a periodic net with the subsequent construction of the natural tiling for the net and generation of TPSs/TPMSs from the faces of the tiles. The TPMSs were classified into nine topological types, three of which were previously unreported. The surfaces were optimized through smoothing and finite-thickness procedures and deposited in a database together with their topological descriptors. Being designed for practical applications, the surfaces are provided in formats compatible with additive manufacturing and standard software tools. Based on some TPMSs, we fabricated periodic porous samples and experimentally showed that they can possess better mechanical properties than the corresponding bulky material. This work expands the repertoire of known minimal surfaces and bridges the gap between micro- and macrostructures in materials design and fabrication. The relations between atomic crystalline architectures and materials with regular structure including metamaterials support the ideas of generalized crystallography disseminated by Alan Mackay long ago (Struct Chem 13:215–220, 2022).

Keywords Crystal structure · Metal-organic framework · Triply periodic minimal surface · Natural tiling

Introduction

The problem of developing an efficient method for constructing triply periodic surfaces (TPSs) including surfaces with zero mean curvature (known as triply periodic minimal surfaces, TPMSs) has a long history and is studied across various branches of mathematics [1–7] and crystallography [8–13]; however, it remains unsolved [5]. This problem took on special significance with the progress of additive manufacturing technologies, which enabled the application of TPS/TPMS structures for the design of porous, composite, and metamaterials across diverse industrial sectors including mechanical engineering, construction, and biomedicine [14, 15]. Materials based on TPS/TPMS structures exhibit intriguing mechanical [16–21], acoustic [22], hydrodynamic, and thermal conductive properties [23–25], along with energy absorption capabilities [26, 27]. Among composite materials that can be fabricated using additive manufacturing methods based on TPSs/TPMSs, we highlight the so-called interpenetrating phase composites [28].

The progress in this field of materials science is significantly hindered by the limited number of known TPS/TPMS structures suitable for additive manufacturing. In practice, the literature predominantly utilizes a very restricted set of TPSs/TPMSs with schwarzites being a prime example of widely employed structures [15]. This scarcity requires generating new TPS/TPMS types. However, current approaches to the TPS/TPMS generation typically modify existing analytically defined surfaces, which fundamentally limit the ability to create surfaces with novel topological architectures [29].

Since TPSs/TPMSs possess three-periodic symmetry, they were of special interest for crystallographers [8–13]. An approach was proposed [30] to utilize natural triply periodic architectures and crystal structures, as templates for

✉ Vladislav A. Blatov
blatov@topospro.com

[1] Samara Center for Theoretical Materials Science, Samara State Technical University, Samara 443100, Russia

[2] Research Laboratory of Computational Geometry and Theoretical Materials Science, Povolzhskiy State University of Telecommunications and Informatics, Samara 443010, Russia

Published online: 10 October 2025

constructing TPSs/TPMSs. Although these ideas were not developed for a long time, they fitted naturally into the concept of generalized crystallography disseminated by Alan Mackay [31].

Recently [32], we developed a novel efficient method for generating TPS/TPMS structures. Our approach combines a network topological representation of periodic structures [33] and their mathematical description through natural tiling theory [34]. In [32], we implemented this method into the ToposPro software package [35] and applied it to derive 98 distinct TPSs including four novel TPMSs using 253 zeolitic atomic networks as templates [36]. We also developed innovative techniques for surface smoothing, thickness control, and format optimization for 3D printing compatibility and integration with standard engineering software packages [37].

Some other approaches to constructing TPSs/TPMSs based on the analysis of periodic networks were proposed in recent years. In [38], TPSs were constructed as electron density isosurfaces, which required additional DFT calculations. Another study [39] utilized crystallographic methods involving Voronoi diagrams and Delaunay triangulation for deriving TPSs from networks. This approach, however, can only generate periodic structures in two dimensions.

In the present study, we apply the methodology developed in [32] to analyze the topological structure of metal-organic frameworks (MOFs) and generate novel TPSs/TPMSs based on the MOF architectures. Through this analysis, we have developed a comprehensive database of TPSs derived from MOF atomic networks, including topological characteristics of the TPSs. Our investigation encompassed 923 MOF structures, from which we identified 131 TPMSs of particular interest. Furthermore, we fabricated several triply periodic porous structures utilizing the TPSs and studied their mechanical properties.

Theoretical background, objects, and computational details

Method

We use the concept of *net*, i.e., a periodic graph which determines the connectivity of atoms and structural groups in a crystal structure. The net nodes coincide with atoms or centers of polyatomic clusters. The edges of the net connect adjacent nodes; if the nodes coincide with atoms, the edges correspond to interatomic contacts; otherwise, the edges mimic linkers between the structural groups whose centers coincide with the net nodes. In the latter case, the whole structure is represented in a simplified way as an underlying net [40] and such representation enables one to establish common structural motifs in chemically different compounds (Fig. 1) [41, 42]. Rigorous algorithms were developed to determine the net for any crystal substance [35, 43] and arrange the nets into topological types [44]. Topologies of the nets are matched by comparison of sets of topological indices, including coordination sequences, extended point symbols, and vertex symbols [45] with the indices of the reference topological types collected in the databases of the TopCryst system (https://topcryst.com) [46]. Hereafter, to designate the net topologies, we use the three-letter RCSR (Reticular Chemistry Structure Resource) notation [44] and *N*D*n* nomenclature, where *N* is a sequence of coordination numbers of all inequivalent nodes of the net, for example, 3,4,4,4,5,5, or $3,4^3,5^2$; D is the net periodicity (M, C, L, or T for finite (molecular), chain, layer, or three-periodic graphs respectively); *n* enumerates topologies with a given *N*D [47].

The general idea of our method is to generate TPSs from periodic nets with a rigorous computer algorithm. For this purpose, we use the *tiling* model [48], which represents the crystal space as a partition by generalized

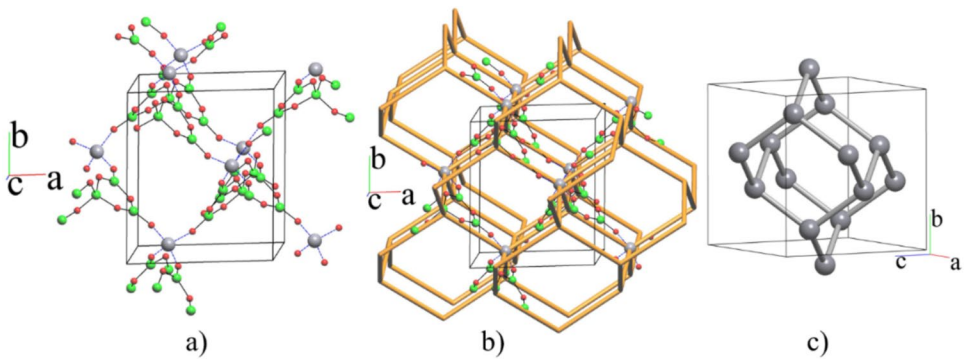

Fig. 1 An example of diamond-like (RCSR symbol **dia**) motifs in the crystal structure of $(Hen)_2[Al(B_5O_{10})]$ (en = ethylenediamine, TOBQIN; hereafter the Cambridge Structural Database (CSD) reference codes are used to designate crystal structures): **a** initial net (Al, B, and O are colored in gray, green, and red, respectively); **b** initial net and the corresponding simplified net (orange sticks) with the **dia** topology; **c** a fragment (adamantane-like cage) of the diamond net

polyhedra (*tiles*). Each tile corresponds to a cage and is confined by rings (tile faces) of the net nodes; each ring mimics the sections of channels between the pair of tiles (cages). Tiles are not necessarily convex and can contain two-coordinated nodes thus having curved faces. Tiles do not intersect each other and share the whole faces, filling the crystal space without gaps. In a natural tiling [49], (natural) tiles represent minimal closed regions which contain neither atoms nor bonds. The natural tile faces are the so-called *strong rings*, i.e., the rings which cannot be split into smaller rings; thus, a natural tile cannot be divided into smaller cages.

The advantages of the natural tiling approach are as follows [49]:

a) The natural tiling approach provides a systematic method for dividing the crystal space, following a standardized procedure. This approach is independent of the net complexity.
b) The natural tiling approach provides insights into potential building units, which can be represented as tiles.
c) The natural tiles correspond to actual minimal cages within the structure; any larger cage can be constructed as a sum of natural tiles.

However, this approach has certain limitations:

a) Some networks do not admit a single natural tiling, but rather allow multiple topologically similar tilings. Usually, this takes place when some large cages can be split to smaller cages in several independent ways. In such cases, all allowable tilings should be considered.
b) The natural tiling and the corresponding atomic network must be three-periodic.
c) The catenated structures, which contain knots of net rings, are mostly not considered in the natural tiling model (some exceptions were discussed in [50, 51]).

A comprehensive algorithm for constructing natural tiling from any three-periodic net was developed and implemented in the ToposPro program package [35]. If an atomic net admits tiling, the *dual net* can be constructed, i.e., the net whose nodes correspond to the centers of natural tiles and edges cross the tile faces. The dual net characterizes the topology of the free space in an atomic network.

Our method for generating TPSs from a natural tiling is based on the following criteria [32]:

(i) *Decoration* criterion*:* the net that admits the natural tiling must fully cover (decorate) the TPS. This condition ensures the surface being triply periodic and interconnected since natural tiling and the corresponding net must be three-periodic.
(ii) *Edge* criterion: the TPS is formed by a set of natural tile faces (strong rings); each edge of the net is shared by exactly two faces from the set. Thus, the resulting TPS has a facet structure; each facet corresponds to a tile face. This condition ensures the surface being 2D and not self-intersected through edges, but requires the removal of some tile faces. As a result of such removal, the labyrinths are formed, which follow the edges of the corresponding dual net.
(iii) *Vertex* criterion: each pair of tile faces from the set, which meet at the same node (vertex) of the net, must share exactly one edge, that is adjacent to that node. This condition ensures that the surface does not intersect itself in a node. In combination, (ii) and (iii) guarantee the absence of any self-crossing of the surface.

As follows from the edge criterion, labyrinth nets can be obtained by splitting the dual net, when only the dual net edges are kept that cross the rings confining the removed tile faces. Thus, we assume that (a) if labyrinth nets A and B are equivalent, the surface is isomorphic to a balanced TPMS; otherwise, it is isomorphic to an unbalanced TPS, which is not necessarily minimal, and (b) if A and B are inequivalent, but A is dual to B and vice versa, the surface is isomorphic to an unbalanced TPMS.

In addition, the type of interweaving of the labyrinth nets can be determined by constructing their Hopf ring nets (HRNs), i.e., the nets whose nodes coincide with the centers of the initial net rings and edges connect the centers of catenated rings [52]. If HRNs of the labyrinth nets of a pair of TPSs are isomorphic, then the labyrinth nets are equivalently interweaved.

If two different nets possess the same labyrinth net, they also have the same genus, i.e., the number of tori that forms the primitive cell of a triply periodic surface, which coincides with the genus of the corresponding TPMS [13]. The genus (g) of any periodic net can be calculated as $g = e - v + 1$, where e and v are, respectively, the numbers of edges and nodes (vertices) in a primitive cell of the net [53].

Thus, the following labyrinth net conditions can be applied to identify the generated TPS:

(i) If the TPS is isomorphic to a TPMS, then there are mutually dual labyrinth nets (MDLNs) tracing the labyrinth.
(ii) If the MDLNs of two TPSs have the same topology, and their HRNs are isomorphic, the surfaces are isomorphic.
(iii) If MDLNs are self-dual, the TPS is isomorphic to a balanced TPMS; otherwise, it is isomorphic to an unbalanced TPMS.

(iv) MDLNs have the same genus *g*, which is equal to the genus of the TPS.

Objects

We analyzed a total of 923 MOF structures and obtained 966 simplified nets including nets obtained by different types of simplification (Tables 1, S1). The initial crystallographic information on the MOFs was taken from the Cambridge Structural Database (CSD); the structures obeyed the following criteria:

(i) *porosity* criterion: theoretical porosity of the MOF should be more than 60% to ensure high porosity of the resulting TPS.
(ii) *periodicity* criterion: metal-organic coordination groups should be three-periodic since only three-periodic net admits a tiling from which TPSs can be generated.

The studied MOFs were quite diverse in their space symmetry (Tables 2, S2) and framework topology (Tables 3, S3).

Computational details

In [32], we used zeolites as porous objects for generating TPSs. In this work, we use other porous structures, MOFs, as templates, which chemically differ from zeolites. The overall generation algorithm includes additional steps, which account for these differences:

(i) Deleting interstitial solvent molecules from the framework.
(ii) Simplifying the framework by cluster or standard methods [41]. The cluster simplification isolates polynuclear complex groups (for example, paddlewheel complexes of copper) and replaces them with the nodes of the simplified net. In the standard simplification, one considers metal atoms and ligands as nodes of the simplified net.
(iii) If the structure contains several interpenetrating frameworks [54], removing all of them but one. This step is needed to exclude catenation, which forbids the construction of natural tiling.
(iv) Removing all one- and two-coordinated nodes from the simplified net. Such nodes cannot participate in the tiling.
(v) Optimizing the resulting net with the Gavrog Systre package [55] to obtain the highest-symmetry embedding of the net. Some nets are discarded at this stage since their topological features do not allow finding the highest-symmetry embedding. In particular, if different nodes of the net share the same barycentric position, Systre fails. For example, the crystal structure of $Zn_3(TATB)_2(H_2O)_2$•4DMF•6H_2O (TATB = 4,4′,4″-s-triazine-2,4,6-triyltribenzoate) cannot be analyzed with Systre, since its simplified **cys**

Table 1 Numbers of nets and triply periodic surfaces at different steps of the algorithm

Total number of initial MOFs	Total number of three-periodic simplified nets	Number of nets after Systre optimization	Total number of generated TPSs	Total number of distinct TPSs/TPMSs	Total number of distinct TPMSs
923	966	881	1601	327	131

Table 2 The most abundant space groups (more than 10 entries) of MOFs

Space group	Number of MOFs	Space group	Number of MOFs	Space group	Number of MOFs
$Fm\bar{3}\,m$	130	$I4/m$	21	$P4_2/mmc$	12
$P2_1/c$	48	$R3m$	21	$P2_12_12_1$	11
$C2/c$	47	$P6/mmm$	15	$Fddd$	11
$R\bar{3}$	47	$I432$	15	$R32$	11
$I\bar{4}\,3\,m$	31	$P4_132$	14	$R\bar{3}\,m$	11
$R\bar{3}\,c$	27	$Pa\bar{3}$	13	$I\bar{4}\,3d$	11
$P\bar{1}$	21	$Im\bar{3}\,m$	13	$Ia\bar{3}\,d$	11

Table 3 The most abundant topologies (more than 10 entries) of simplified nets in MOFs

Topology	Number of MOFs	Topology	Number of MOFs	Topology	Number of MOFs
pcu	100	**pts**	37	**nbo**	15
tbo	62	**srs**	37	**eea**	14
4,8T1	52	**nts**	28	**fcu**	13
dia	40	**rtl**	27	**lvt**	12
sod	39	**flu**	15		

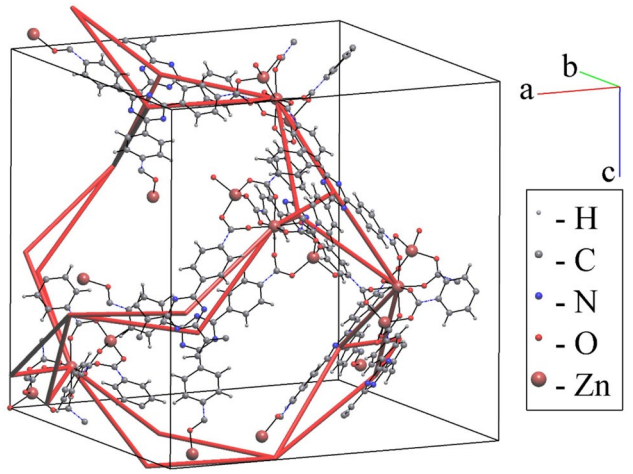

Fig. 2 The metal-organic framework of $Zn_3(TATB)_2(H_2O)_2$•4DMF•6H_2O (PIBNUK) [56] with the complete and simplified nets. Hereafter, the simplified net is represented by red cylinders

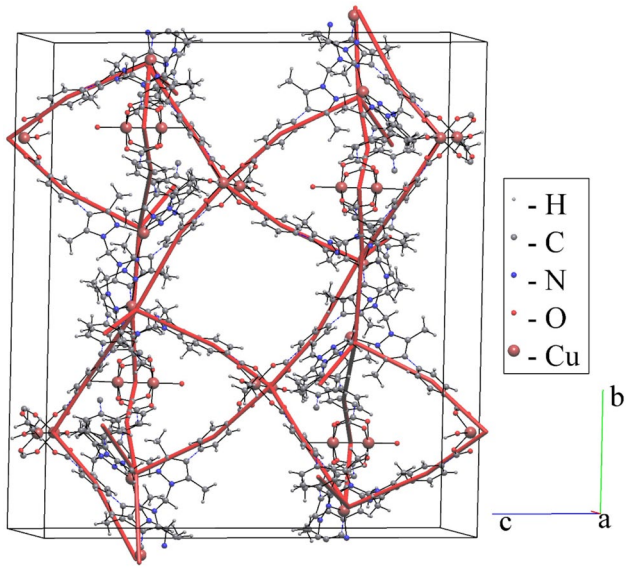

Fig. 3 The metal-organic framework of $Cu_4[Cu^I(\mathbf{bcpdmpm})_2]_2(EtOH)_2(H_2O)_2\}(NO_3)_2$•12DMF ($H_2$**bcpdmpm** = bis(4-carboxyphenyl)−3,5-dimethyl-1*H*-pyrazolyl) methane, AGOFEJ) [57] does not admit natural tiling

net has collisions between next-nearest nodes (Fig. 2). Thus, such nets are not suitable as TPS templates.

(vi) Constructing natural tilings and the corresponding dual nets according to the algorithm [35]. At this stage, the MOFs are discarded, which do not admit natural tiling (Fig. 3).

(vii) Successive removal of strong rings (natural tile faces) from the initial set, and verifying the decoration, edge, and vertex criteria for each resulting subset of the rings. Some MOFs do not fit these criteria and should also be excluded from the subsequent analysis (Fig. 4). As a result, only 52 MOFs served as templates for TPSs.

(viii) Generating the corresponding labyrinth nets from the dual net by removing the nodes intersecting the surface facets (Fig. 5).

(ix) Determining the topological properties of the labyrinth nets including their number, periodicity, topological type, genus, and HRN for each potential TPS.

(x) Using the properties of the labyrinth nets to determine whether the TPS is isomorphic to a TPMS, whether it is novel and balanced. For practical use, the resulting facet surfaces can then be smoothed (see below).

The surface geometry generated by this method depends on how tile faces are represented. In ToposPro, faces are modeled as triangulated polygons, resulting in a piecewise-planar approximation composed of triangular facets. This triangulated mesh serves as a linear interpolation of the underlying smooth surface. To better approximate a true minimal surface, further smoothing is required to minimize mean curvature across all points, progressively converging toward the minimal surface equation [5]:

$$\operatorname{div}\left[\nabla u\left(1+|\nabla u|^2\right)^{-1/2}\right]=0 \tag{1}$$

where $u = u(x, y)$ is the minimal surface function.

A hybrid smoothing algorithm that combines the advantages of different smoothing approaches while mitigating their limitations was proposed in [32]. Our method uses the average dihedral angle between facets as a key metric while simultaneously minimizing local mean curvature. The optimization process follows this principle: the difference between maximum and minimum mean curvature values across all mesh vertices should be minimized. For the calculation of the discrete mean curvature at each vertex, we employ the normal cycles theory framework from differential geometry [61], which provides a robust mathematical foundation for curvature estimation on polyhedral surfaces:

$$\Phi^H(B)=\sum_{e\in E}\text{length}(e\cap B)\beta(e) \tag{2}$$

where B is a sphere with a radius equal to the shortest edge in the surface mesh; E is the set of the mesh edges e; $\beta(e)$ is the angle between the normals to the facets; $\beta(e)$ is positive if e is convex and negative if e is concave; length($e \cap B$) is the length of a great circle intersection of sphere B and edge e (Fig. 6).

This approach enables us to

- maintain geometric fidelity through dihedral angle optimization

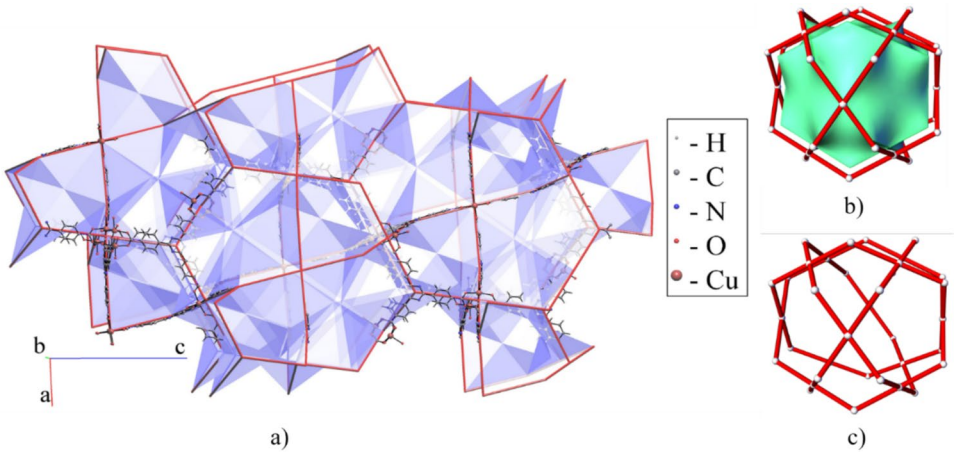

Fig. 4 $Cu_3(TATB)_2(H_2O)_3$ (TATB = 4,4′,4″-*s*-triazine-2,4,6-triyltribenzoate, ACUFEK) [58, 59] is shown as the complete and simplified nets (**a**). Removal of the strong rings from the $[6^8.8^6]$ tiles of the simplified net (**b**) results in disappearing of any surface (**c**) and impossibility to construct a labyrinth net

- achieve near-minimal surface properties through curvature equalization
- preserve the topological constraints of the original TPS structure

The developed smoothing algorithm shows comparable or better results than the widely used Surface Evolver [62]. The complete algorithmic implementation and mathematical details of the smoothing procedure are provided in [32].

Results and discussion

Using the approach described above, we generated 131 TPMSs from the 923 MOF structures (Table S4). We determined the numbers and topology of their labyrinth nets and found nine topologically distinct TPMSs whose labyrinth nets are non-isomorphous (Table S5). Eight of them appeared to be isomorphic with previously known TPMSs, while three can be considered isomorphic to novel unbalanced TPMSs (Table 4). To distinguish new surfaces, we used the notation **g*ABCDEF_X, where *g* represents the surface genus, ABCDEF is the MOF CSD six-letter reference code, and X is the serial number of the surface obtained from the origin ABCDEF MOF.

The *9HEJGAI TPS is characterized by the 4,6,8-coordinated **kty** and 3,4,12T41 labyrinth nets (Fig. 7). These nets are not MDLN; while 3,4,12T41 is dual to **kty**, the dual of 3,4,12T41 is the 4,5,6T195 net, which can be transformed to **kty** by squeezing two 5-coordinated nodes to an 8-coordinated node. Thus, *9HEJGAI is a geometrically distorted unbalanced TPMS.

The *18YUSWEP TPS has 4,24-coordinated **twf** and 6,8-coordinated **ocu** labyrinth nets (Fig. 8). The **twf** and **ocu** as well are not MDLN; thus, neither **twf** nor **ocu** is dual of each other. The dual of **twf** is **twf-d**, which can be transformed to **ocu** by squeezing two 12-coordinated atoms to a 24-coordinated. The simplification scheme is similar to the **ocu** labyrinth net – the dual of **ocu** is **xag**, which can be transformed to **twf** by contracting a 3-coordinated node. Hence, *18YUSWEP is also a geometrically distorted unbalanced TPMS.

On the contrast, the *13SAPBIW TPS is characterized by the 5-coordinated **lcs** and 4-coordinated **gan** labyrinth nets, which are MDLN (Fig. 9). Hence, *13SAPBIW is an unbalanced TPMS.

Along with the novel three-periodic surfaces, a pair of D-type TPS complementary or disphenoid surfaces [62] was discovered (Fig. 10). Constructed from two different sets of strong rings, such surfaces are topologically identical and have 4-coordinated **dia** and 3,6-coordinated **llw-z** labyrinth nets.

The generated TPS/TPMSs can be used to fabricate new porous materials for various engineering purposes. For example, in [20], we investigated the mechanical properties of 15 triply periodic P-surfaces (Fig. 9) derived from zeolite atomic frameworks using numerical simulations in the ANSYS package. These surfaces can also be obtained from MOFs (Table 5).

Interestingly, the structures from Table 5 enabled the generation of 15 TPSs that closely match the geometric and topological features of Schwarz P-surfaces. The resulting TPSs fall into three subclasses (Table 5, Fig. 11). The P class comprises surfaces that strictly follow the Schwarz classification, while $\widetilde{P}$ (P-like) surfaces exhibit a similar structure but can undergo deformations such as compression or stretching. The $\widetilde{P_D}$ (P-disp) surfaces, though topologically identical to P-surfaces, possess different unit cells because they are extracted from varying segments of the same infinite triply periodic structure and can also experience transformations.

The porous structures exhibited pronounced anisotropic behavior, with maximum stiffness observed under z-axis compression. The compression moduli, shear moduli, and

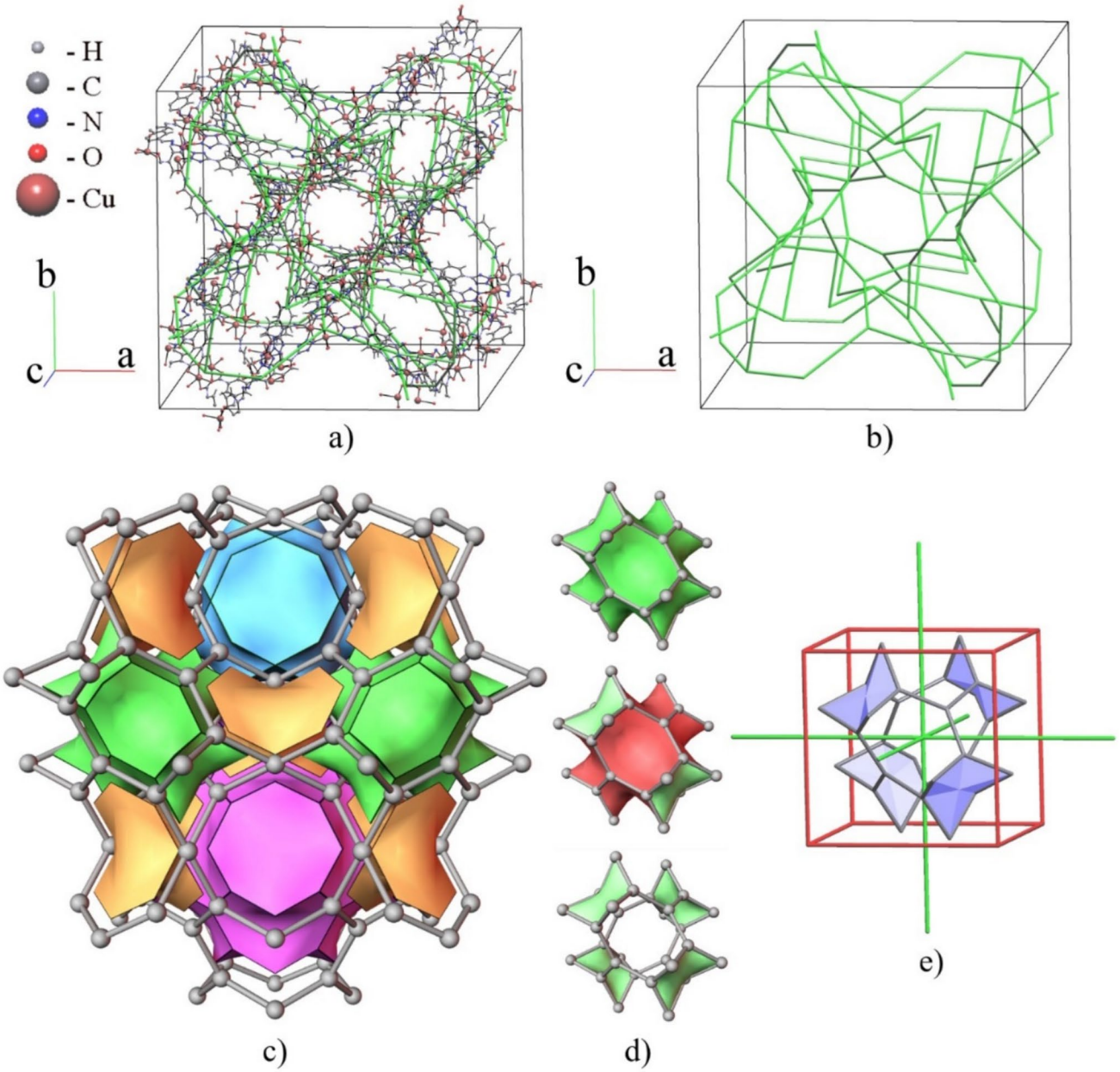

Fig. 5 The metal-organic framework and natural tiling in the crystal structure of $[Cu_6O(L4)_3(NO_3)\cdot xsolv]_n$ ($H_3L4 = 5'$-(4-(1*H*-tetrazol-5-yl)benzamido)benzene-1,3-dioic acid, ADATIK) [60]: **a** atomic triply periodic net and the corresponding simplified net highlighted in green; **b** the simplified net with the **ntt** topology; **c** the natural tiling together with the simplified net highlighted in gray; **d** a tile (top), six red 8-membered faces, which need to be removed to form the channels (center), the tile with removed faces (bottom); **e** the tile with the removed faces and the corresponding labyrinth nets represented as two independent channel systems highlighted in red and green

Poisson's ratios were computed under multidirectional loading, revealing significant variations across different configurations. The materials derived from CGF and HEU demonstrated extreme anisotropy, with z-axis moduli up to 100 times higher than transverse values.

Von Mises stress distribution analysis showed generally uniform stress patterns, though some structures, such as derived from ITW and LAU, exhibited localized high-stress concentrations. The BRE-derived material stood out with exceptionally low stress concentrations, suggesting favorable load distribution. The study also applied the Gibson-Ashby scaling law to relate mechanical properties to relative density, confirming linear scaling behavior. This indicated that the performance of these structures remained consistent across varying densities, making them suitable for applications requiring predictable mechanical responses.

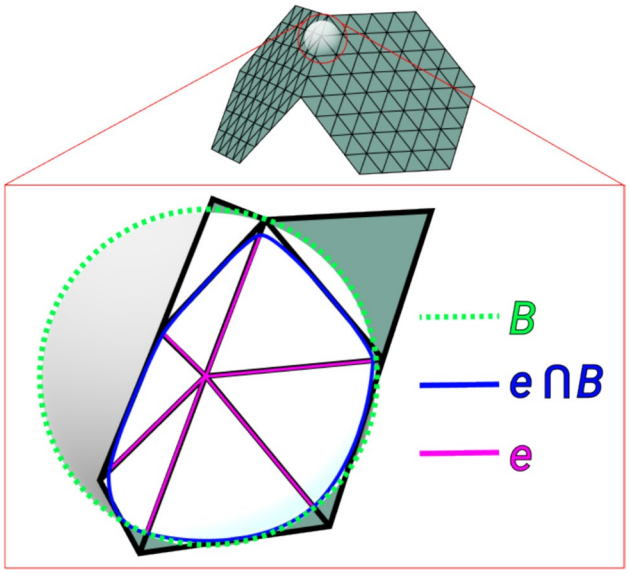

Fig. 6 Calculation of discrete mean curvature employs a spherical neighborhood (green dotted sphere) with radius r equal to the shortest mesh edge length. Purple lines display the original surface, while blue lines represent the optimized smoothed version. The curvature is computed using normal cycles theory and accounting for local dihedral angles and contributions from neighboring vertices

Based on the findings from the unit cell analysis, we extended our investigation to larger-scale porous structures assembled from CGF, HEU, and SAS unit cells. We simulated these structures using ANSYS software Finite Element modeling with the specific mechanical properties of PLA+ filament to accurately predict how the 3D-printed structures would behave under stress [18, 20]. Finite element simulations incorporated nonlinear mechanics to capture plastic deformation, ensuring accurate predictions of mechanical behavior under compressive loading.

Stress distribution analysis revealed distinct failure mechanisms between the structures. CGF- and HEU-based materials exhibited stress concentrations at boundary regions, leading to progressive failure, while SAS-based structures experienced internal stress concentrations, resulting in abrupt structural collapse. Notably, some configurations, particularly HEU and CGF, demonstrated yield and ultimate strengths exceeding those of the base PLA+ material by up to 13.5%. This strengthening effect was attributed to the low stress concentrations within internal regions of the structures, which delayed failure initiation.

An experimental validation confirmed the computational predictions, reinforcing the potential of these porous structures for applications where enhanced mechanical performance is critical. The findings highlight the importance of topological design in optimizing load-bearing capacity and failure resistance in engineered porous materials. Future research of porous structures based on

Table 4 Topological characteristics of the three new TPMSs

TPMS name	Simplified net topology	MOF formula	Strong rings*	Space group	Labyrinth net topology #1	Number of nodes	Coordination of nodes	Labyrinth net topology #2	Number of nodes	Coordination of nodes
*13SAPBIW	4,6T117	$Zn_8(ad)_4(BPDC)_6O_2$; $4Me_2NH_2$, 49DMF, $31H_2O$ (ad = adeninate, BPDC = biphenildicarboxylate, Me = methyl)	4b,5a	$Ia\bar{3}\,d$	**gan**	1	5	**lcs**	1	4
*18YUSWEP	4^4T152	$Cu_2(H_2O)_2$(PMTB) (PMTB = diphenylmethane-3,3′,5,5′-tetrakis(3,5-bisbenzoate)	4a,4b,6e,8d,8i	$Im\bar{3}\,m$	**ocu**	2	6, 8	**twf**	2	4, 24
*9HEJGAI	4^7T38	$[Cu_6(C_s\text{-mdip})_2(C_{2v}\text{-mdip})\text{-}(H_2O)_6]\cdot 3DMA\cdot 6H_2O$ (mdip = 5,5′- methylene-di-isophthalate, DMA = dimethylacetamide)	4a,4b,8 g,8 h,8n,8r	*P4/mmm*	**kty**	3	4, 6, 8	3,4,12T41	3	3, 4, 12

*Size of the ring and symmetry code are given

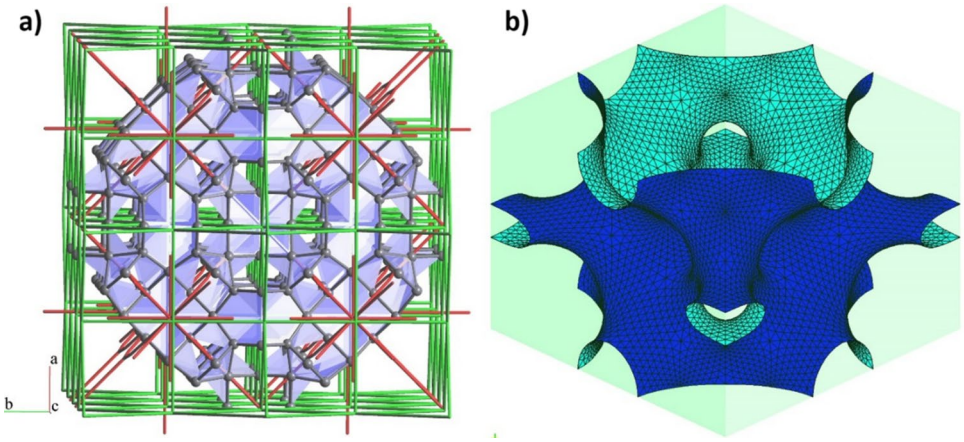

Fig. 7 A novel *9HEJGAI TPS: **a** the facets (blue) and the labyrinth nets **kty** (red) and 3,4,12T41 (green); **b** smoothed *9HEJGAI TPS

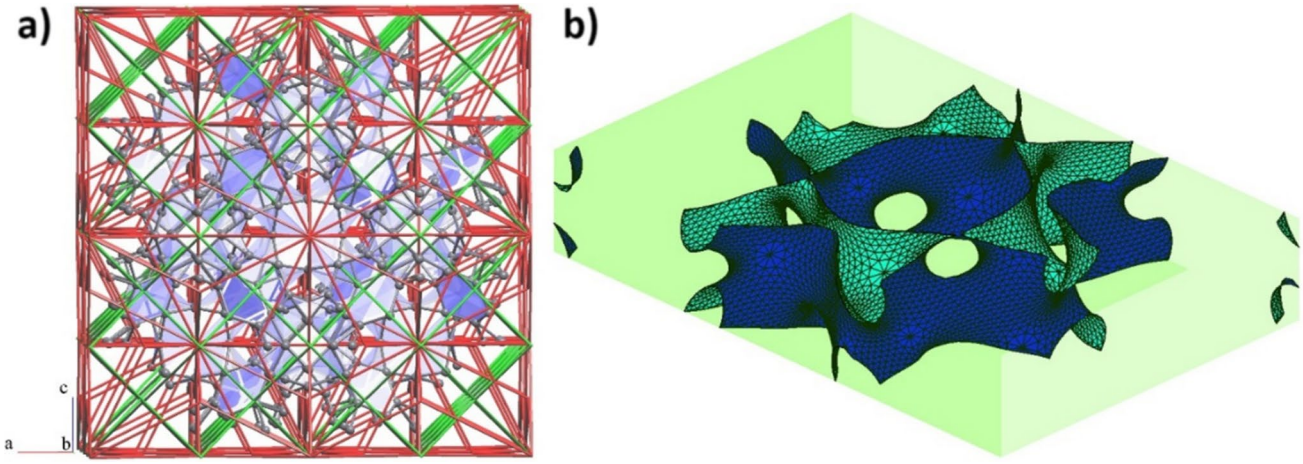

Fig. 8 A novel *18YUSWEP TPS: **a** the facets (blue) and labyrinth nets **twf** (red) and **ocu** (green); **b** smoothed *18YUSWEP TPS

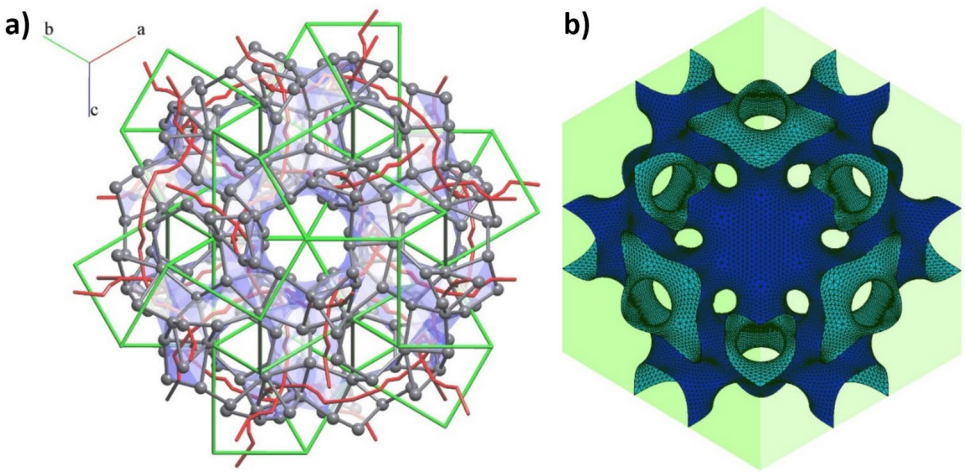

Fig. 9 A novel *13SAPBIW TPMS: the facets (blue) and labyrinth nets **gan** (red) and **lcs** (green); **b** smoothed *13SAP-BIW TPMS

TPSs/TPMSs derived from MOFs could explore additional geometric variations and material combinations to further refine these structures for specific industrial or biomedical applications.

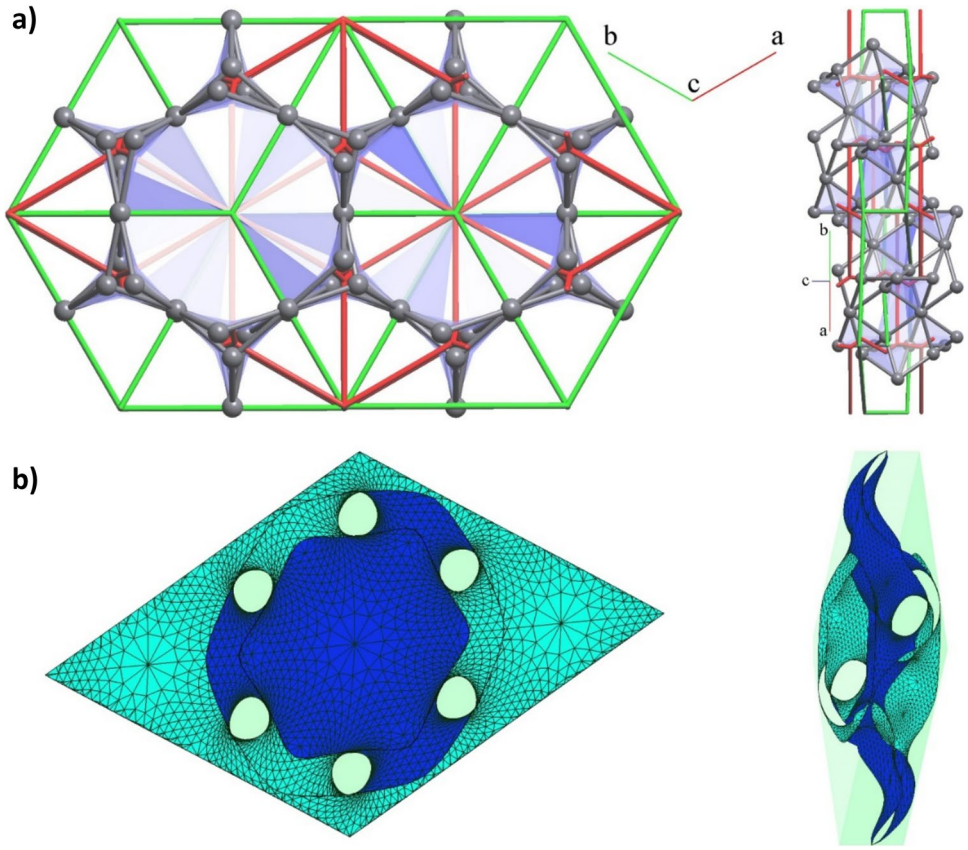

Fig. 10 A TPS complementary surface constructed from $Co_2(dobdc)\cdot 2CH_4$ ($dobdc^{4-}$ = 2,5-dioxido-1,4-benzenedicarboxylate, VAMQOS): **a** the facets (blue) and labyrinth nets **dia** (red) and **llw-z** (green); **b** smoothed sample of this TPS

Table 5 Schwarz P-surfaces subclassification by their geometrical parameters

P-type	Zeolites (Fig. 9)	Examples of MOFs
P	SOD (Sodalite), RHO (Rhodenite)	BAZFUF, FAWCEN, OFERUN02, YIBZOC, ZEQYON, MINMAA, NIFNOI
P-like ($\widetilde{P}$)	ATN (MAPO-39), LTA (Linde Type A)	IZEPAF, VEJYIT
P-disp ($\widetilde{P_D}$)	BCT (Mg-BCCT), MER (Merlinoite), SAS (STA-6), UEI (Mu-18), BRE (Brewsterite), EDI (Edingtonite), ITW (ITQ-12), LAU (Laumontite), CGF (Cobalt-Gallium-Phosphate-5), HEU (Heulandite), JSW (CoAPO-CJ62)	ADASAB, ADASEF, ADATIK, ZIZBAO

Concluding remarks

This study presents a systematic and efficient method for generating TPSs and TPMSs from MOFs, expanding the repertoire of known minimal surfaces and their applications in materials science. By leveraging topological representations and natural tiling theory, we analyzed 923 MOF structures and identified 131 TPMSs, which belong to nine topological types, three of which were previously unreported. The surfaces were further optimized through advanced smoothing algorithms and finite-thickness procedures, ensuring compatibility with additive manufacturing and standard engineering software.

Our findings highlight the versatility of MOFs as templates for generating novel TPSs/TPMSs, with applications spanning mechanical engineering, biomedicine, and energy absorption. The study also underscores the importance of topological analysis in materials design, as demonstrated by the ability of different MOF structures to produce identical surfaces. Furthermore, the practical utility of these surfaces was illustrated through the fabrication of periodic porous structures, showcasing their potential for tailored mechanical and functional properties.

This work not only advances the theoretical understanding of minimal surfaces but also provides a comprehensive, annotated database of TPS/TPMS structures,

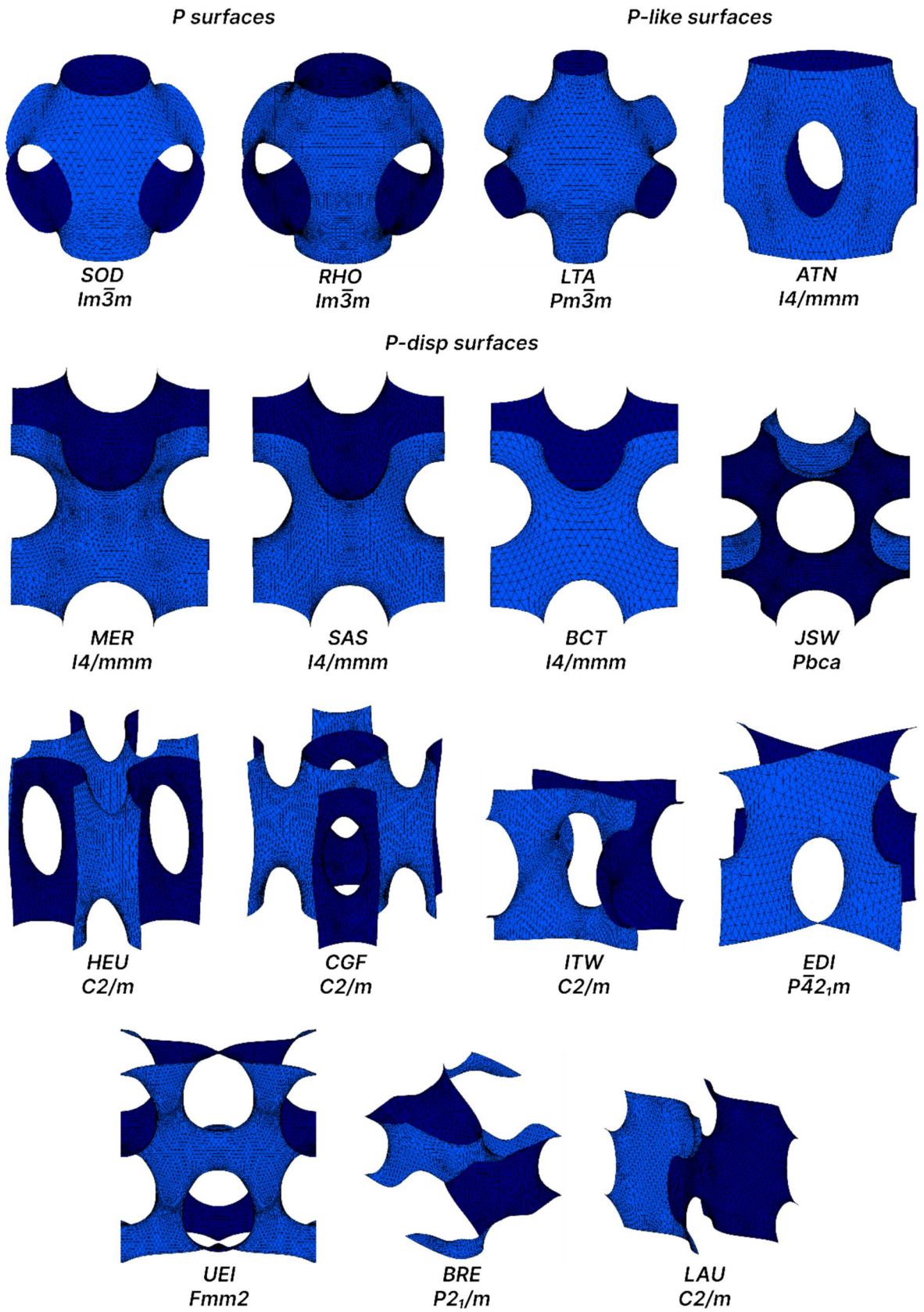

Fig. 11 15 triply periodic P-surfaces named after the corresponding zeolite templates (Table 5)

which can serve as a valuable resource for future research and industrial applications. Future studies could explore additional geometric variations, material combinations, and scaling effects to further optimize these structures for specific engineering and biomedical needs. The methodologies and insights presented here pave the way for innovative applications of TPSs/TPMSs in the design of next-generation materials and develop Alan Mackay's ideas of generalized crystallography.

Supplementary Information The online version contains supplementary material available at https://doi.org/10.1007/s11224-025-02631-2.

Acknowledgements We thank an anonymous referee for valuable comments that helped us to improve the manuscript.

Author contribution M.I.S. performed smoothing approximation of the generated surfaces, E.O.B. generated triply periodic surfaces from natural tiling of MOFs, E.D.B. performed topological classification of the labyrinth nets, A.F.K. and V.A.B. wrote the main part of the manuscript. All authors reviewed the manuscript.

Funding This work was supported by the Russian Science Foundation, grant 25-13-00076.

Data availability Supporting Information file with the list of all 923 CSD reference codes of MOFs, topological parameters of 131 generated TPMSs and nine topological types of TPMSs.

Declarations

Ethics approval All authors approve the ethics guidelines.

Consent to participate All authors agree to participate in this work.

Consent for publication All authors agree to publish this work as a journal paper.

Competing interest The authors declare no competing interests.

References

1. Osserman R (1967) Minimal surfaces Russian Math Surveys 22:55–136
2. Schoen A (1970) Infinite periodic minimal surfaces without self-intersections. National Aeronautics and Space Administration, Washington, DC, NASA Technical Report TN D-5541
3. Karcher H, Polthier K (1996) Construction of triply periodic minimal surfaces. Philos Trans R Soc Lond Ser A Math Phys Eng Sci 354:2077–2104. https://doi.org/10.1098/rsta.1996.0093
4. Schoen AH (2012) Reflections concerning triply-periodic minimal surfaces. Interface Focus 2:658–668. https://doi.org/10.1098/rsfs.2012.0023
5. Pérez J (2017) A new golden age of minimal surfaces. Notices Am Math Soc 64:347–358. https://doi.org/10.1090/noti1500
6. Mackay AL, Terrones H (1991) Diamond from graphite. Nature 352:762–762. https://doi.org/10.1038/352762a0
7. Yin M, Zhang J, Vvedensky DD (2025) Density-functional theory and triply-periodic minimal surfaces. Phys Rev Mater 9:073802. https://doi.org/10.1103/trld-8v8h
8. Koch E, Fischer W (1988) On 3–periodic minimal surfaces with non–cubic symmetry. Z Kristallogr Cryst Mater 183:129–152. https://doi.org/10.1524/zkri.1988.183.14.129
9. Fischer W, Koch E (1989) New surface patches for minimal balance surfaces. I. Branched catenoids. Acta Crystallogr A 45:166–169. https://doi.org/10.1107/S0108767388010797
10. Koch E, Fischer W (1989) New surface patches for minimal balance surfaces. Part II. Multiple catenoids. Acta Crystallogr A 45:169–174. https://doi.org/10.1107/S010876738801075X
11. Fischer W, Koch E (1989) New surface patches for minimal balance surfaces. III. Infinite strips. Acta Crystallogr A 45:485–490. https://doi.org/10.1107/S010876738900317X
12. Koch E, Fischer W (1989) New surface patches for minimal balance surfaces. IV. Catenoids with spout-like attachments. Acta Crystallogr A 45:558–563. https://doi.org/10.1107/S0108767389003648
13. Fischer W, Koch E (1989) Genera of minimal balance surfaces. Acta Crystallogr A 45:726–732. https://doi.org/10.1107/S0108767389006616
14. Günther F, Pilz S, Hirsch F, Wagner M, Kästner M, Gebert A, Zimmermann M (2023) Shape optimization of additively manufactured lattices based on triply periodic minimal surfaces. Addit Manuf 73:103659. https://doi.org/10.1016/j.addma.2023.103659
15. Felix LC, Ambekar R, Tromer RM, Woellner CF, Rodrigues V, Ajayan PM, Tiwary CS, Galvao DS (2025) Schwarzites and triply periodic minimal surfaces: from pure topology mathematics to macroscale applications. Small 21:2400351. https://doi.org/10.1002/smll.202400351
16. Lin Z-H, Pan J-H, Li H-Y (2022) Mechanical strength of triply periodic minimal surface lattices subjected to three-point bending. Polymers (Basel) 14:2885. https://doi.org/10.3390/polym14142885
17. Li Z, Chen Z, Chen X, Zhao R (2023) Mechanical properties of triply periodic minimal surface (TPMS) scaffolds: considering the influence of spatial angle and surface curvature. Biomech Model Mechanobiol 22:541–560. https://doi.org/10.1007/s10237-022-01661-7
18. Eremin AV, Frolov MA, Krutov AF, Smolkov MI, Shulga AS, Bragin DM, Popov AI, Blatov VA (2024) Mechanical properties of porous materials based on new triply periodic and minimal surfaces. Mech Adv Mater Struct 31:11320–11336. https://doi.org/10.1080/15376494.2024.2303724
19. Wang Y, Lian Y, Wang Z, Wang C, Fang D (2024) A novel triple periodic minimal surface-like plate lattice and its data-driven optimization method for superior mechanical properties. Appl Math Mech 45:217–238. https://doi.org/10.1007/s10483-024-3079-7
20. Frolov MA, Smolkov MI, Krutov AF, Burchakov AV, Blatov VA (2025) Comparative analysis of mechanical properties of porous structures obtained on the basis of triply periodic P-surfaces. Mech Adv Mater Struct 1–18. https://doi.org/10.1080/15376494.2025.2518468
21. Gaal V, Felix LC, Woellner CF, Galvao DS, Tiwary CS, d'Ávila MA, Rodrigues V (2022) Mechanical properties of 3D printed macroscopic models of schwarzites. Nano Select 3:450–458. https://doi.org/10.1002/nano.202100147
22. Silva T, Lu J-Y, Abu Al-Rub RK, Lee D-W (2024) Investigation on tailoring the width and central frequency of bandgaps of TPMS structures. Int J Mech Mater Des 20:317–329. https://doi.org/10.1007/s10999-023-09677-2
23. Yeranee K, Rao Y (2022) A review of recent investigations on flow and heat transfer enhancement in cooling channels embedded with triply periodic minimal surfaces (TPMS). Energies (Basel) 15:8994. https://doi.org/10.3390/en15238994
24. Xia Q, Zhu J, Yu Q, Kim J, Li Y (2024) Triply periodic minimal surfaces based topology optimization for the hydrodynamic and

convective heat transfer. Commun Nonlinear Sci Numer Simul 131:107819. https://doi.org/10.1016/j.cnsns.2024.107819
25. Eremin AV, Frolov MA, Krutov AF, Smolkov MI, Bragin DM, Popov AI (2025) Experimental and numerical study of thermal and mechanical properties of porous materials based on triply periodic surfaces. Materials and Solidification 1:9580001. https://doi.org/10.26599/MAS.2025.9580001
26. Wallat L, Selzer M, Wasmuth U, Poehler F, Nestler B (2022) Energy absorption capability of graded and non-graded sheet-based gyroid structures fabricated by microcast processing. J Mater Res Technol 21:1798–1810. https://doi.org/10.1016/j.jmrt.2022.09.093
27. Wang Z, Chen B, Lu Y, Zhou J, Li D, Yue D, Zhang X (2024) Mechanical properties and energy absorption of medium-entropy alloy triply periodic minimal surface cellular structures fabricated via selective laser melting. Mech Mater 196:105084. https://doi.org/10.1016/j.mechmat.2024.105084
28. Khedri E, Karimi H, Aliha MRM, Nazemzadeh N, Talebi B, Aleali R (2024) Tensile, flexural, and mode-I cracking behavior of interpenetrating phase composites (IPC), developed using additively manufactured PLA-based structures with different infill densities and epoxy resin polymer as matrix. Results Eng 22:102162. https://doi.org/10.1016/j.rineng.2024.102162
29. Xu Y, Pan H, Wang R, Du Q, Lu L (2023) New families of triply periodic minimal surface-like shell lattices. Addit Manuf 77:103779. https://doi.org/10.1016/j.addma.2023.103779
30. Andersson S, Hyde ST, Schnering VHG (1984) The intrinsic curvature of solids. Z Kristallogr Cryst Mater 168:1–18. https://doi.org/10.1524/zkri.1984.168.14.1
31. Mackay AL (2002) Generalized crystallography. Struct Chem 13:215–220. https://doi.org/10.1023/A:1015838303255
32. Smolkov MI, Blatova OA, Krutov AF, Blatov VA (2022) Generating triply periodic surfaces from crystal structures: the tiling approach and its application to zeolites. Acta Crystallogr A Found Adv 78:327–336. https://doi.org/10.1107/S2053273322004545
33. Delgado-Friedrichs O, Foster MD, O'Keeffe M, Proserpio DM, Treacy MMJ, Yaghi OM (2005) What do we know about three-periodic nets? J Solid State Chem 178:2533–2554. https://doi.org/10.1016/j.jssc.2005.06.037
34. Anurova NA, Blatov VA, Ilyushin GD, Proserpio DM (2010) Natural tilings for zeolite-type frameworks. J Phys Chem C Nanomater Interfaces 114:10160–10170. https://doi.org/10.1021/jp1030027
35. Blatov VA, Shevchenko AP, Proserpio DM (2014) Applied topological analysis of crystal structures with the program package ToposPro. Cryst Growth Des 14:3576–3586. https://doi.org/10.1021/cg500498k
36. Baerlocher Ch, McCusker LB, Olson DH (2007) Atlas of zeolite framework types, 6th edn. Elsevier, Amsterdam. https://doi.org/10.1016/B978-0-444-53064-6.X5186-X
37. Porous 3D documentation release 1.0.1. TopCryst (n.d.) https://p3d.topcryst.com/software/. Accessed 17 Aug 2025
38. Arsentev MYu, Sysoev EI, Makogon AI, Balabanov SV, Sychev MM, Hammouri MH, Moshnikov VA (2023) High-throughput screening of 3D-printed architected materials inspired by crystal lattices: procedure, challenges, and mechanical properties. ACS Omega 8:24865–24874. https://doi.org/10.1021/acsomega.3c00874
39. Castañeda FD, García-Acosta G, Garzón-Alvarado DA, Márquez-Flórez K, Quexada-Rodriguez DA, Velasco MA (2024) Design for the additive manufacturing of structural elements with cellular materials using Voronoi diagrams and Delaunay triangulations: biological and structural applications. Mech Adv Mater Struct 31:9550–9570. https://doi.org/10.1080/15376494.2023.2276837
40. Alexandrov EV, Blatov VA, Kochetkov AV, Proserpio DM (2011) Underlying nets in three-periodic coordination polymers: topology, taxonomy, and prediction from a computer-aided analysis of the Cambridge Structural Database. CrystEngComm 13:3947. https://doi.org/10.1039/c0ce00636j
41. Shevchenko AP, Blatov VA (2021) Simplify to understand: how to elucidate crystal structures? Struct Chem 32:507–519. https://doi.org/10.1007/s11224-020-01724-4
42. Bonneau C, O'Keeffe M, Proserpio DM, Blatov VA, Batten SR, Bourne SA, Lah MS, Eon J-G, Hyde ST, Wiggin SB, Öhrström L (2018) Deconstruction of crystalline networks into underlying nets: relevance for terminology guidelines and crystallographic databases. Cryst Growth Des 18:3411–3418. https://doi.org/10.1021/acs.cgd.8b00126
43. Blatov VA, Proserpio DM (2010) Periodic-graph approaches in crystal structure prediction. In: Oganov AR (ed) Modern methods of crystal structure prediction. Wiley, Weinheim, pp 1–28. https://doi.org/10.1002/9783527632831.ch1
44. O'Keeffe M, Peskov MA, Ramsden SJ, Yaghi OM (2008) The reticular chemistry structure resource (RCSR) database of, and symbols for, crystal nets. Acc Chem Res 41:1782–1789. https://doi.org/10.1021/ar800124u
45. Blatov VA, O'Keeffe M, Proserpio DM (2010) Vertex–, face–, point–, Schläfli–, and Delaney–symbols in nets, polyhedra and tilings: recommended terminology. CrystEngComm 12:44–48. https://doi.org/10.1039/B910671E
46. Shevchenko AP, Shabalin AA, Karpukhin IYu, Blatov VA (2022) Topological representations of crystal structures: generation, analysis and implementation in the TopCryst system. Sci Technol Adv Mater Methods 2:250–265. https://doi.org/10.1080/27660400.2022.2088041
47. Blatov VA, Alexandrov EV, Shevchenko AP (2021) Topology: ToposPro. In: Constable EC, Parkin G, Que Jr. L (eds) Comprehensive coordination chemistry III. Elsevier, Oxford, pp 389–412. https://doi.org/10.1016/B978-0-12-409547-2.14576-7
48. O'Keeffe M (1999) Tiling by numbers. Nature 400:617–618. https://doi.org/10.1038/23139
49. Blatov VA, Delgado-Friedrichs O, O'Keeffe M, Proserpio DM (2007) Three-periodic nets and tilings: natural tilings for nets. Acta Crystallogr A 63:418–425. https://doi.org/10.1107/S0108767307038287
50. Bonneau C, O'Keeffe M (2015) High-symmetry embeddings of interpenetrating periodic nets. Essential rings and patterns of catenation. Acta Crystallogr A Found Adv 71:82–91. https://doi.org/10.1107/S2053273314019950
51. Delgado-Friedrichs O, O'Keeffe M, Proserpio DM, Treacy MMJ (2023) Three-periodic nets, tilings, and surfaces. A short review and new results. Acta Crystallogr A Found Adv 79:192–202. https://doi.org/10.1107/S2053273323000414
52. Alexandrov EV, Blatov VA, Proserpio DM (2012) A topological method for the classification of entanglements in crystal networks. Acta Crystallogr A 68:484–493. https://doi.org/10.1107/S0108767312019034
53. de Campo L, Delgado-Friedrichs O, Hyde ST, O'Keeffe M (2013) Minimal nets and minimal surfaces. Acta Crystallogr A 69:483–489. https://doi.org/10.1107/S0108767313018370
54. Carlucci L, Ciani G, Proserpio DM (2003) Polycatenation, polythreading, and polyknotting in coordination network chemistry. Coord Chem Rev 246:247–289. https://doi.org/10.1016/S0010-8545(03)00126-7
55. Delgado-Friedrichs O, O'Keeffe M (2003) Identification of and symmetry computation for crystal nets. Acta Crystallogr A 59:351–360. https://doi.org/10.1107/S0108767303012017
56. Sun D, Ke Y, Collins DJ, Lorigan GA, Zhou H-C (2007) Construction of robust open metal–organic frameworks with chiral channels and permanent porosity. Inorg Chem 46:2725–2734. https://doi.org/10.1021/ic0624773

57. Bloch WM, Doonan CJ, Sumby CJ (2013) Using hinged ligands to target structurally flexible copper(II) MOFs. CrystEngComm 15:9663. https://doi.org/10.1039/c3ce41244j
58. Sun D, Ma S, Ke Y, Collins DJ, Zhou H-C (2006) An interweaving MOF with high hydrogen uptake. J Am Chem Soc 128:3896–3897. https://doi.org/10.1021/ja058777l
59. Ma S, Sun D, Ambrogio M, Fillinger JA, Parkin S, Zhou H-C (2007) Framework-catenation isomerism in metal–organic frameworks and its impact on hydrogen uptake. J Am Chem Soc 129:1858–1859. https://doi.org/10.1021/ja067435s
60. Eubank JF, Nouar F, Luebke R, Cairns AJ, Wojtas L, Alkordi M, Bousquet T, Hight MR, Eckert J, Embs JP, Georgiev PA, Eddaoudi M (2012) On demand: the singular rht net, an ideal blueprint for the construction of a metal–organic framework (MOF) platform. Angew Chem Int Ed Engl 51:10099–10103. https://doi.org/10.1002/anie.201201202
61. Cohen-Steiner D, Morvan J-M (2003) Restricted Delaunay triangulations and normal cycle. In: Proceedings of the nineteenth annual symposium on Computational geometry. ACM, New York, NY, USA, pp 312–321
62. Brakke KA (1992) The surface evolver. Exp Math 1:141–165. https://doi.org/10.1080/10586458.1992.10504253